Supporting Information

Ampere-hour-scale soft-package potassium-ion hybrid capacitors enabling 6-minute fast-charging

Huanxin Li,[1, 3, 9] Yi Gong,[2, 9] Haihui Zhou,[1*] Jing Li,[4] Kai Yang,[2] Boyang Mao,[3] Jincan Zhang,[3] Yan Shi,[5] Jinhai Deng,[6] Mingxuan Mao,[7] Zhongyuan Huang,[1] Shuqiang Jiao,[8*] Yafei Kuang,[1] Yunlong Zhao,[2*] Shenglian Luo[1*]

[1] State Key Laboratory for Chemo/Biosensing and Chemometrics, College of Chemistry and Chemical Engineering, Hunan University, Changsha, Hunan, 410082, China

[2] Advanced Technology Institute, University of Surrey, Guildford, Surrey GU2 7XH, United Kingdom

[3] Department of Engineering, University of Cambridge, 9 JJ Thomson Avenue, Cambridge, CB3 0FA, United Kingdom

[4] Department of Chemical & Process Engineering, University of Surrey, Guildford, GU2 7XH, United Kingdom

[5] College of Materials and Metallurgy, Guizhou University, Guiyang 550025, China

[6] King's College London, London, SE1 1UL, United Kingdom

[7] Department of Electrical and Electronic Engineering, Imperial College London, London SW7 2AZ, United Kingdom

[8] State Key Laboratory of Advanced Metallurgy, University of Science and Technology Beijing, Beijing, 100083, China

[9] These authors contributed equally

[*]Correspondence: H.Z.; S.J.; Y.Z.; S.L.

Figures

CV tests for the capacitive behaviours

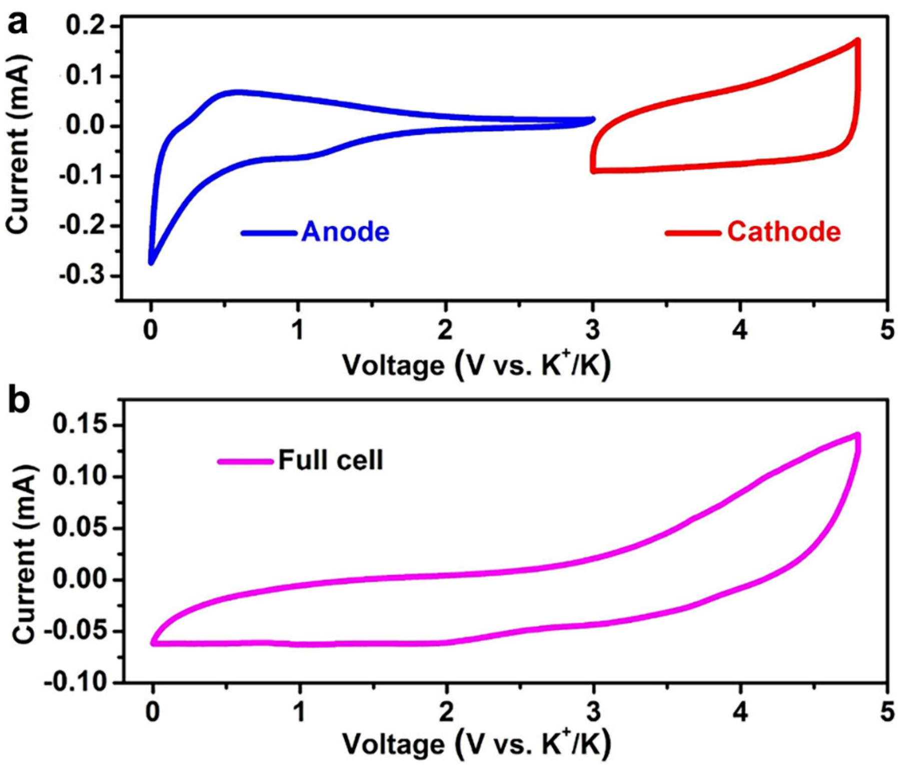

Figure S1. a Schematic of the mechanism for potassium storage in PIBHCD. **b** The relative shapes of CV curves for full cell.

Morphologies of electrodes (Figure S2-S6)

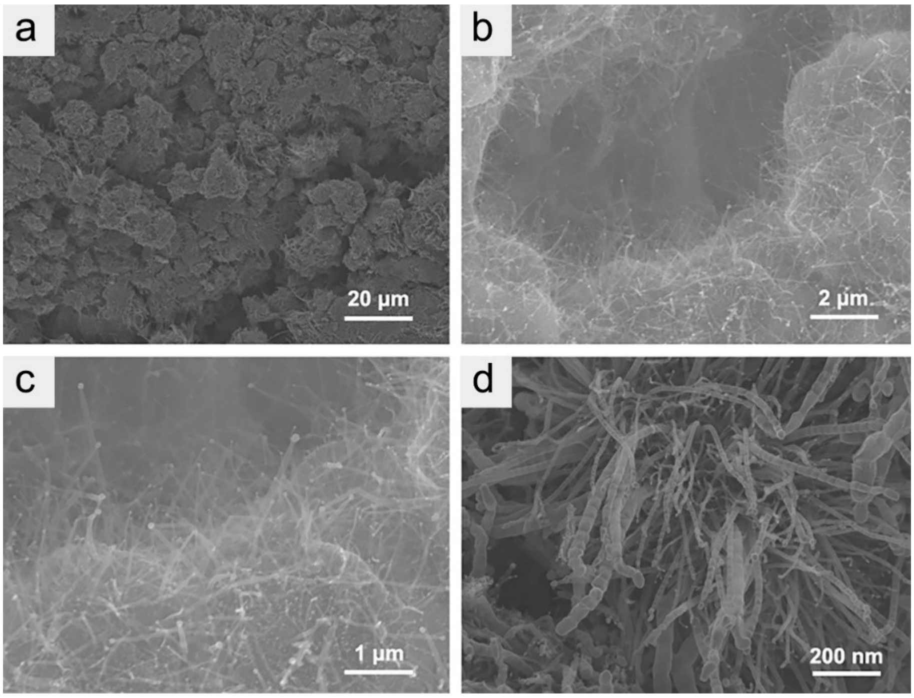

Figure S2. SEM images of Fe_2O_3-CNNTs@MC at different magnification, scale bar: **a** 20 μm. **b** 2 μm. **c** 1 μm. **d** 200 nm.

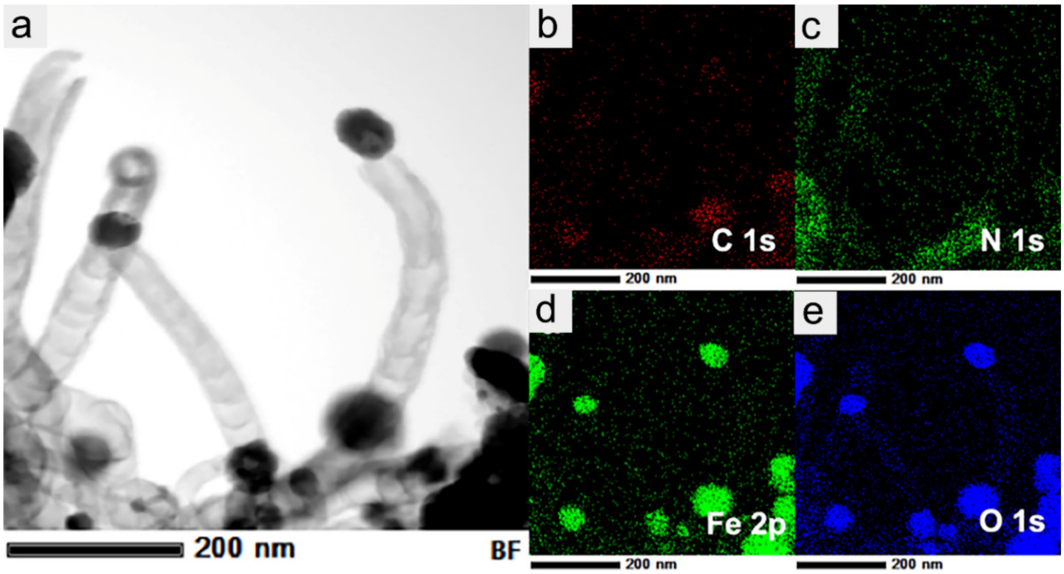

Figure S3. a Typical TEM images of Fe_2O_3-CNNTs@MC and corresponding ma pping images for **b** C, **c** N, **d** Fe and **e** O elements.

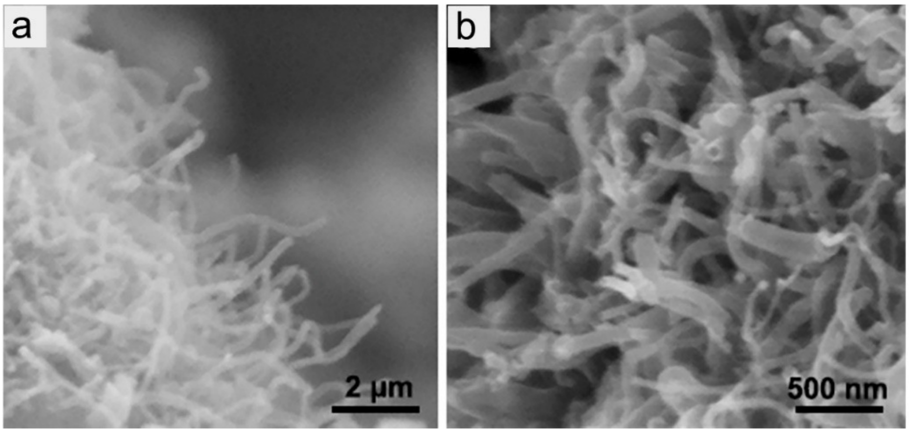

Figure S4. SEM images of N–CNTs@MC after acid wash and high-temperature heat treatment at different magnification, scale bar: **a** 2 μm, **b** 500 nm.

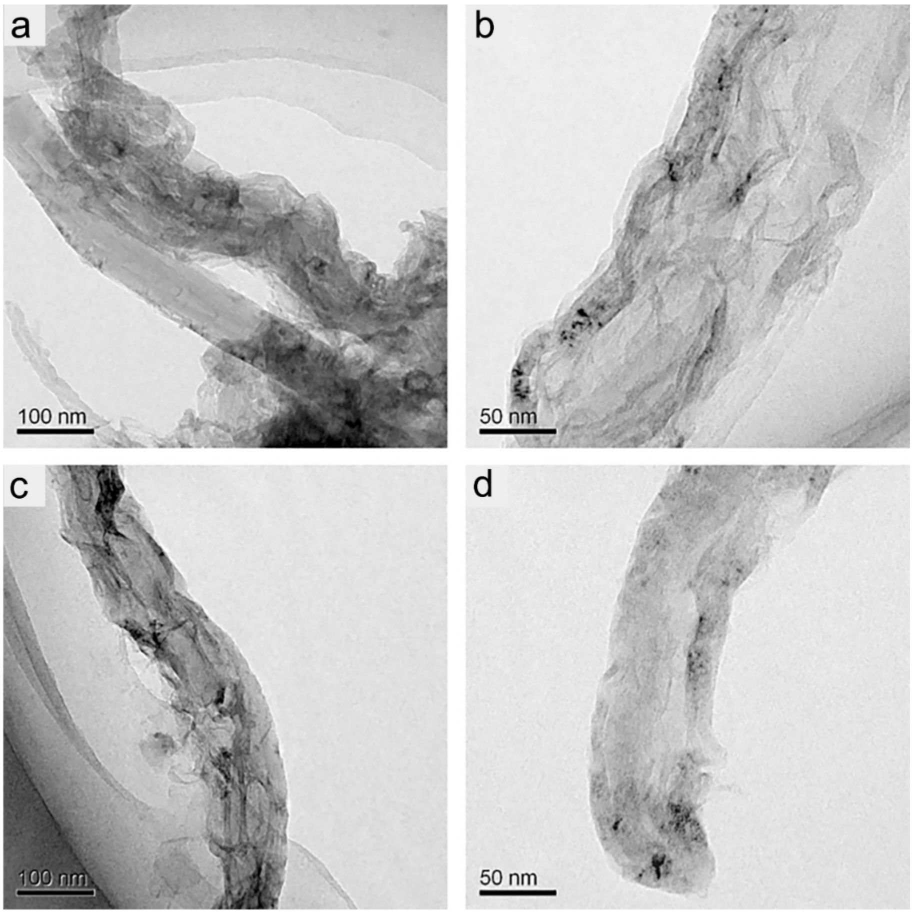

Figure S5. TEM images of the carbon nanotubes in N–CNTs@CMC after acid w ashing.

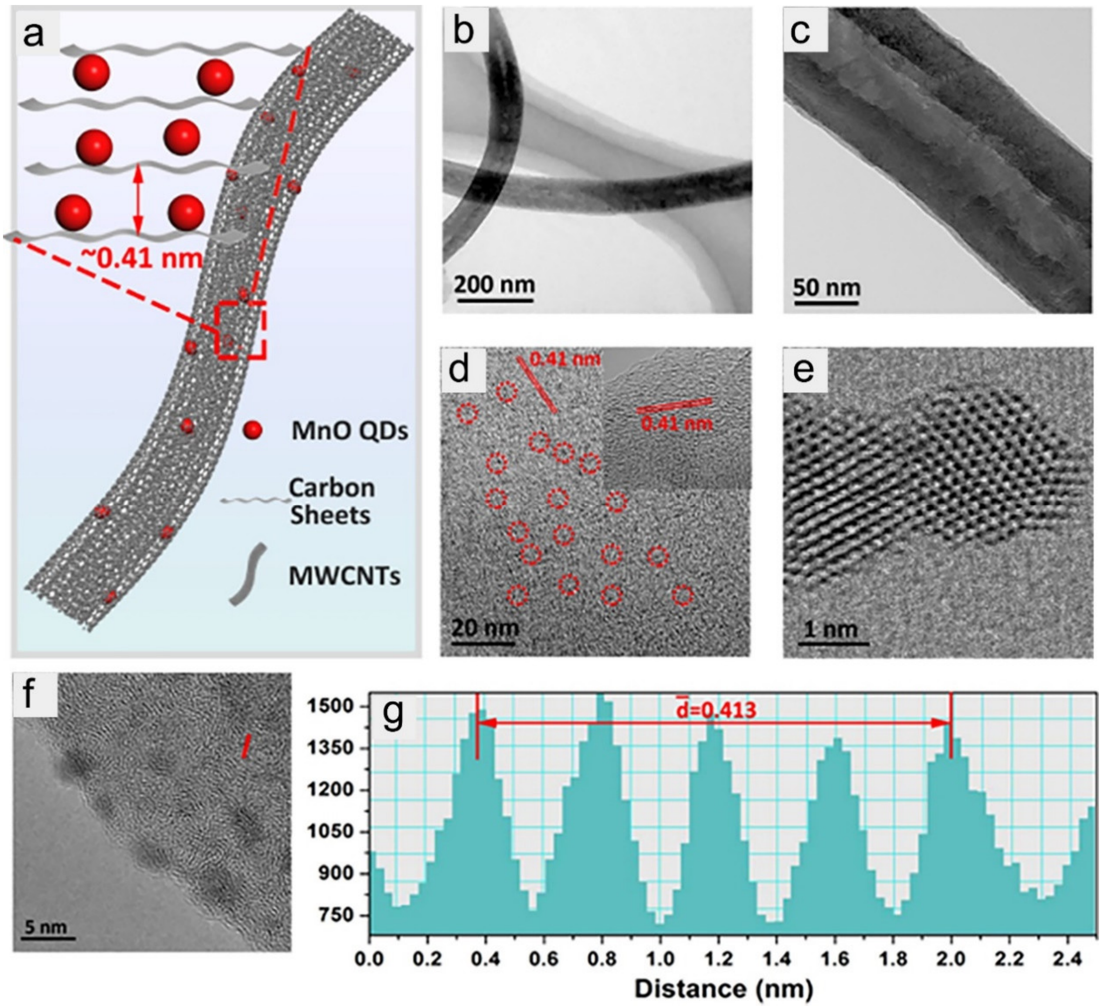

Figure S6. **a** Schematic diagram, **b** TEM and **(C)** enlarged TEM images of MnO QD@CHNTs; **c** High resolution TEM image on the wall of MnOQD@CHNTs; **e** Atomic image of the MnO quantum dots; **f** TEM image of MnOQD@CHNTs wit h clear diffraction fringes of carbon layer and **g** corresponding carbon layer spaci ng.

Compositions and structures (Figure S7-S11)

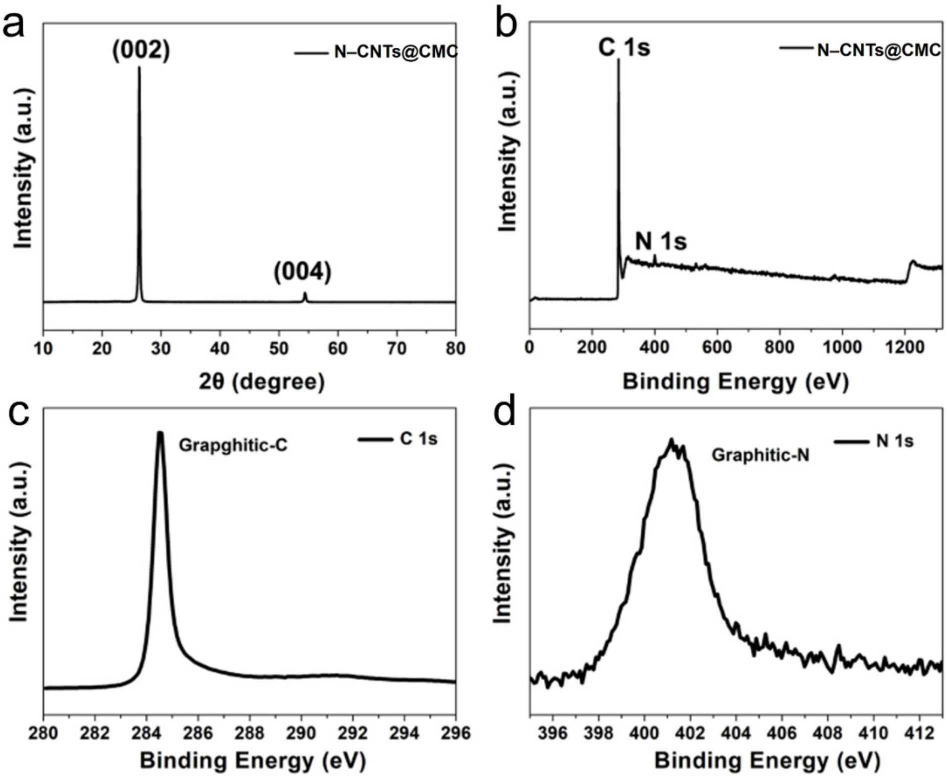

Figure S7. a XRD pattern of N–CNTs@CMC; **b** XPS survey of N–CNTs@CMC; **c** XPS high resolution peaks of C 1s and **d** N 1s in N–CNTs@CMC.

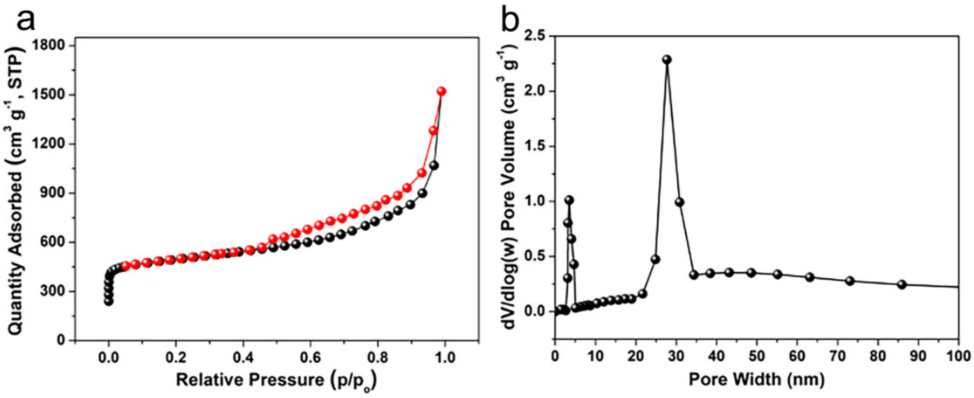

Figure S8. a Nitrogen adsorption-desorption isotherms and **b** pore size distributions of N–CNTs@CMC.

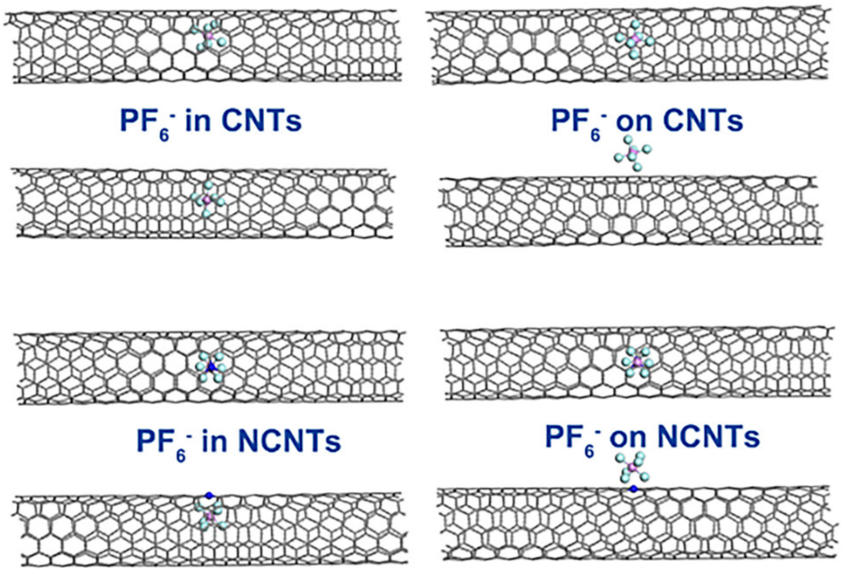

Figure S9. The optimized structures of adsorbed PF_6^- ions on CNT and N-CNT.

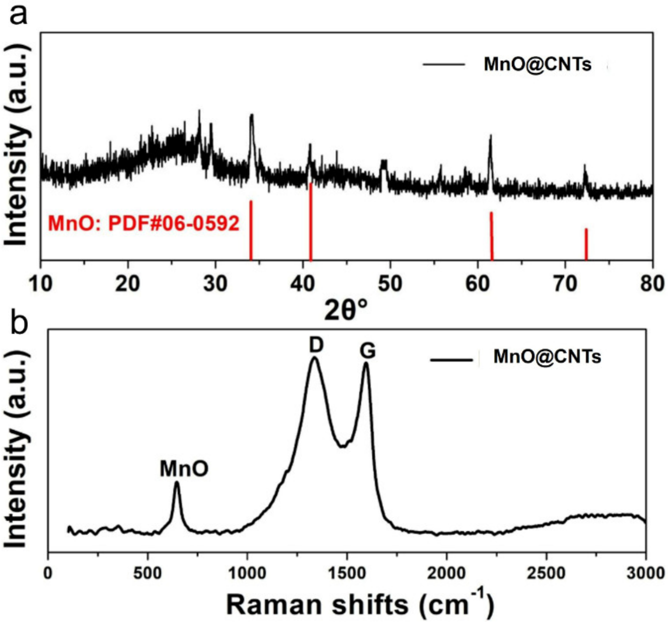

Figure S10. a XRD pattern of MnO@CNTs. **b** Raman spectra of MnO@CNTs.

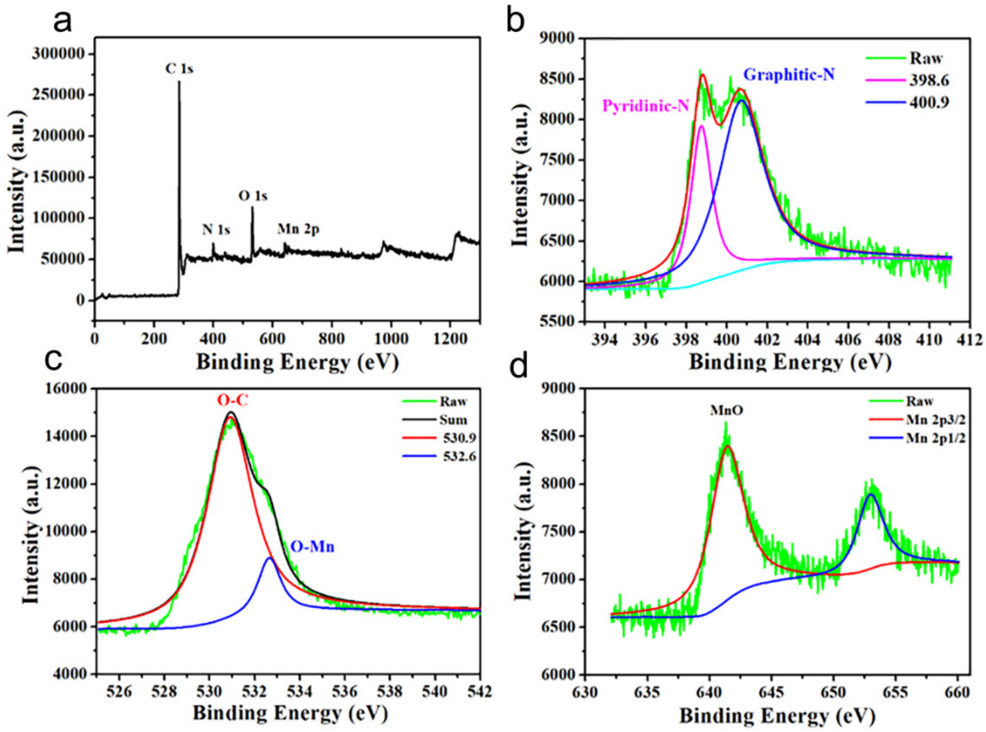

Figure S11. XPS survey of MnO@CNTs.

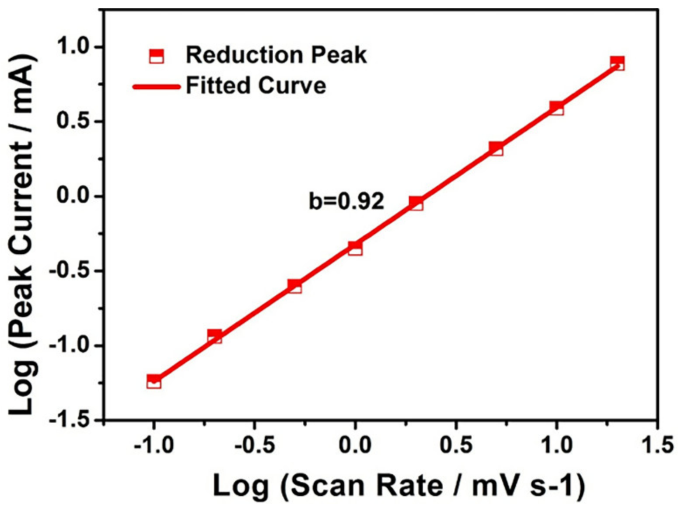

Figure S12. Log(i)–log(v) curves for b-value determination

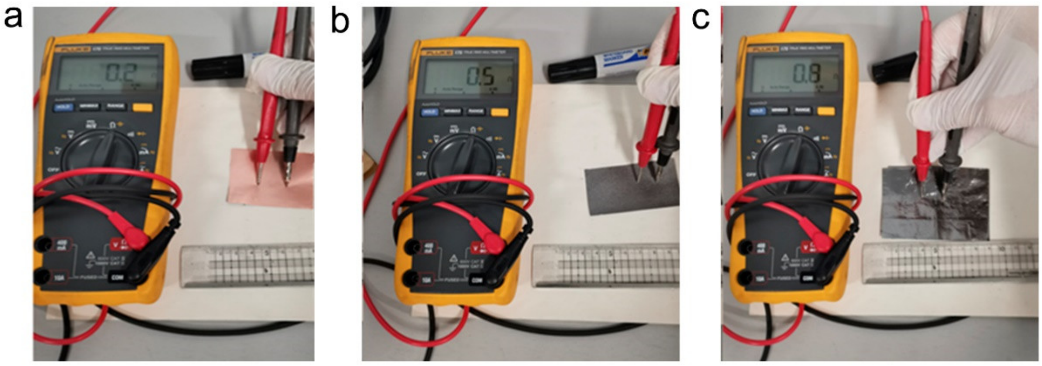

Figure S13 Comparison of the conductivity of **a** Cu foil, **b** N-CNTs@MC film and **c** MnO@CNTs film

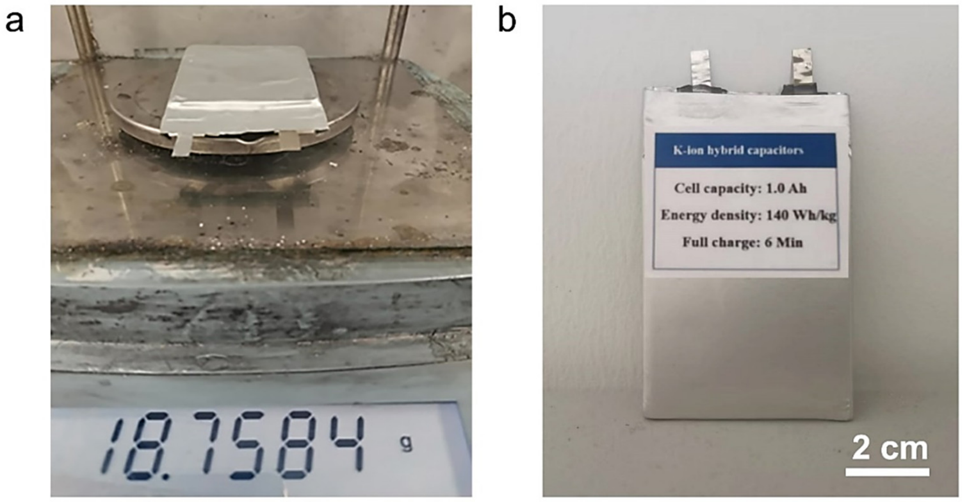

Figure S14. a The weight of ~1Ah PIBHCD. **b** The picture of the prepared 1Ah PIBHCD

Tables

Table S1 Optimized parameters of the soft-packaged PIBHCD with the capacity of ~1Ah

Parameters of winded soft-package PIBHSD						
	Cathode	**Anode**	**Separator**	**S (cm^2)**	**Total V (cm^3)**	**Volume Density (Wh/L)**
Area mass (mg cm^{-2})	30.0	10.0	1.7	Single	7.5	283.2
				24.8		
Thickness (μm	150.0	40.0	12.0	Stack	**Electrolyte (mg)**	**Shell and Tags (mg)**
				10.0	4474.5	3186.4
Denisty (g cm^{-3})	~2.0	~2.5	~1.42	**Core mass**	**Total mass (mg)**	**Energy Density (Wh/Kg)**
Mass (mg)	7425.0	2722.5	950.0	11097.5	18758.4	131.9

Table S2 Free energies from DFT calculations for and PF_6^-, CNTs, NCNTs, PF_6^-@CNTs, PF_6^-@NCNTs, K^+, MnO@G, and K^+on G and K^+on MnO@G

Calculation of adsorption energies (eV)			
PF_6^- on SCNT			
E_{PF6-} (eV)	E_{CNTs} (eV)	$E_{PF6-@CNTs}$ (eV)	$\Delta E_{ads\ (CNTs\text{-}PF6\text{-})}$ (eV)
-30.92	-3103.04	-3136.15	**-2.19**
PF_6^- on NCNT			
E_{PF6-} (eV)	E_{NCNTs} (eV)	$E_{PF6-@NCNTs}$ (eV)	$\Delta E_{ads\ (NCNTs\text{-}PF6\text{-})}$ (eV)
-30.92	-3107.30	-3148.42	**-10.21**
K^+ on G			
E_{K+} (eV)	E_{G} (eV)	$E_{K+@G}$ (eV)	$\Delta E_{ads\ (NCNTs\text{-}PF6\text{-})}$ (eV)
-2.36	-526.32	-529.94	**-1.26**
K^+ on MnO@G			
E_{k+} (eV)	$E_{MnO@G}$ (eV)	$E_{K+@MnO@G}$ (eV)	$\Delta E_{ads\ (NCNTs\text{-}PF6\text{-})}$ (eV)
-2.36	-690.95	-698.08	**-4.76**

Table S3 Comparison with the recently-reported representative PIBHCD

Cathode//Anode[Ref.]	**Voltage (V)**	**Energy density (Wh kg^{-1})**	**Power density (W kg^{-1})**	**Type of devices**
N-CNTs@MC//MnO@CNTs **[Our work]**	0.8-4.8	**140** Wh kg^{-1} (based on the whole weight of PIBHCD);	1400 W kg^{-1} (10 C, fully charged within **6** mins)	**1Ah Pouch cell**
FCDAC//CNS[1]	0-4.2	40 (based on the weight of the electrode)	21000	coin cell
ANHCS//NHCS[2]	0.01-4	19.1	8203	coin cell
3DNFC//3DNFAC[3]	1.5-4.2	76.4	21000	coin cell
WS_2@NCN//NCHS[4]	0.6-4.2	103.4	235	coin cell
AC//$Ca_{0.5}Ti_2(PO_4)_3$@C[5]	1-4	34	5144	coin cell
U-Co_2P@rGO-14//AC[6]	1-4	87	4260	coin cell
AC//Sn[7]	1-4	120	2850	2-layer pouch cell
AC//SC[8]	0-4	120	599	coin cell
KTO//NGC[9]	0-3.5	58.2	7200	coin cell
WPCS//WPCS[10]	0-4.5	44	15400	coin cell
AC//$MoSe_2$/C-700[11]	1-4	106	588	coin cell
AC//NMCP@rGO[12]	0.01-4.2	63.6	19091	coin cell
AC//$NbSe_2$/NSeCNFs[13]	0.01-4	145	/	coin cell

References

1. Chen J*, et al.* Disordered, large interlayer spacing, and oxygen-rich carbon nanosheets for potassium ion hybrid capacitor. *Advanced Energy Materials* **9**, 1803894 (2019).

2. Qiu D*, et al.* Kinetics enhanced nitrogen-doped hierarchical porous hollow carbon spheres boosting advanced potassium-ion hybrid capacitors. *Advanced Functional Materials* **29**, 1903496 (2019).

3. Yang B*, et al.* 3D nitrogen-doped framework carbon for high-performance potassium ion hybrid capacitor. *Energy Storage Materials* **23**, 522-529 (2019).

4. Li Y*, et al.* Enhanced cathode and anode compatibility for boosting both energy and power densities of Na/K-ion hybrid capacitors. *Matter* **1**, 893-910 (2019).

5. Zhang Z*, et al.* Fast potassium storage in hierarchical Ca0. 5Ti2 (PO4) 3@ C microspheres enabling high-performance potassium-ion capacitors. *Advanced Functional Materials* **28**, 1802684 (2018).

6. Wang Y*, et al.* Ultrafine Co 2 P nanorods wrapped by graphene enable a long cycle life performance for a hybrid potassium-ion capacitor. *Nanoscale Horizons* **4**, 1394-1401 (2019).

7. Lang J, Li J, Ou X, Zhang F, Shin K, Tang Y. A flexible potassium-ion hybrid capacitor with superior rate performance and long cycling life. *ACS applied materials & interfaces* **12**, 2424-2431 (2019).

8. Fan L, Lin K, Wang J, Ma R, Lu B. A nonaqueous potassium-based battery–supercapacitor hybrid device. *Advanced materials* **30**, 1800804 (2018).

9. Dong S, Li Z, Xing Z, Wu X, Ji X, Zhang X. Novel potassium-ion hybrid capacitor based on an anode of K2Ti6O13 microscaffolds. *ACS applied materials & interfaces* **10**, 15542-15547 (2018).

10. Cui Y*, et al.* Bioinspired mineralization under freezing conditions: an approach to fabricate porous carbons with complicated architecture and superior K+ storage performance. *Acs Nano* **13**, 11582-11592 (2019).

11. Shen Q, Jiang P, He H, Chen C, Liu Y, Zhang M. Encapsulation of MoSe 2 in carbon fibers as anodes for potassium ion batteries and nonaq

ueous battery–supercapacitor hybrid devices. *Nanoscale* **11**, 13511-13520 (2019).

12. Ruan J*, et al.* Rational construction of nitrogen-doped hierarchical dual-carbon for advanced potassium-ion hybrid capacitors. *Advanced Energy Materials* **10**, 1904045 (2020).

13. Chen M*, et al.* An Ultrastable Nonaqueous Potassium-Ion Hybrid Capacitor. *Advanced Functional Materials* **30**, 2004247 (2020).